Materials.

Graphite powder, $KMnO_4$, H_2SO_4, HNO_3, HCl, H_2O_2, $Zn(NO_3)_2{\cdot}6H_2O$, 2-methylimidazole (2-MeIM), NaCl, poly(vinylidene fluoride) (PVDF), methanol, and N-methyl-2-pyrrolidinone (NMP) were purchased from Wako Pure Chemical Industries and used without further purification.

Experimental Section.

Synthesis of GO. The synthesis of graphene oxide (GO) was conducted according to a procedure reported by Xu et al.[S1] In brief, graphite powder was put into a solution of concentrated HNO_3 and H_2SO_4 (1:2 by volume) and kept at 80 °C for 5 h. The mixture was cooled to room temperature, diluted with deionized (DI) water, and left overnight. Then, the reaction vessel was immersed in an ice bath, and $KMnO_4$ was added slowly. The mixture was successively stirred and left for 2 h. Then, after dilution with DI water, 30% H_2O_2 was added into the mixture, and the color of the mixture changed to brilliant yellow, which was accompanied by bubbling. Finally, the mixture was filtered and washed with HCl aqueous solution (1:10 in volume), DI, and ethanol, respectively. Finally, the obtained GO was dried in a vacuum oven at 60 °C for 24 h.

Synthesis of ZIF-8/GO. 0.366 g of $Zn(NO_3)_2{\cdot}6H_2O$ and 0.811 g of 2-MeIM were dissolved in 12 and 20 mL methanol, respectively. Then, $Zn(NO_3)_2$ methanolic solution (12 mL) was added into the 2-MeIM methanolic solution to obtain a clear solution. 8 mL of GO solution (1 mg mL^{-1} in water) was immediately added to the above mixed solution. After stirring for 0.5 h, the gray precipitate was collected by centrifugation (6000 rpm for 5 min) and was washed with methanol at least three times. After being dried at 60 °C for 12 h, zeolitic imidazolate framework-8 (ZIF-8)/GO was prepared.

Synthesis of NC/rGO. Nitrogen-doped/reduced graphene oxide (NC/rGO) was obtained via carbonizing ZIF-8/GO at 950 °C for 2 h in N_2 atmosphere. For comparison, reduced graphene oxide (rGO) was obtained via directly carbonizing GO by the same process.

Materials characterization.

Powder X-ray diffraction (XRD) patterns were obtained on an Ultima Rint 2000 X-ray diffractometer (RIGAKU, Japan) using Cu Kα radiation (40 kV, 40 mA, 2 ° min^{-1} scan rate). N_2 adsorption/desorption isotherms were measured using an ASAP 2020 Accelerated Surface Area and Porosimetry System (Micromeritics, Norcross, GA) at 77 K. The surface areas of samples were estimated based on the Brunauer−Emmett−Teller (BET) model by using the adsorption branch data in the relative pressure (P/P_0) range of 0.05−0.3. The pore size distribution profile was obtained by using the Barrett−Joyner−Halenda model. X-ray photoelectron spectroscopy (XPS) measurements were performed on an Imaging Photoelectron Spectrometer (Axis Ultra, Kratos Analytical Ltd.) with a monochromatic Al Kα X-ray source. The overall morphology of the samples was characterized on a Hitachi SU8000 field emission scanning electron microscope (FESEM) operating at 5 kV. Before SEM observations, a platinum coating was applied to ensure clear SEM images. The specific morphology was obtained on a JEOL JEM-2100 field emission transmission electron microscope (TEM).

Electrochemical performance measurements.

For electrode preparation, 80 wt% sample was mixed with 10 wt% carbon black and 10 wt% PVDF in NMP solvent. After ultrasonication for 15 min, a certain volume of the mixture was dropped onto graphite paper (thickness: 1 mm) and dried at 60 °C.

All electrochemical measurements were carried out on a CHI 660E electrochemical workstation. In a three-electrode system, the electrochemical performances of the rGO and NC/rGO electrodes were tested by cyclic voltammetry (CV) in 1 M NaCl as aqueous electrolyte with a platinum wire as the counter electrode and an Ag/AgCl electrode as the reference electrode.

Calculation of specific capacitances derived from the CV curves: In general, the gravimetric capacitance (C_g, F g^{-1}) is calculated using the following equation:

$$C_g = \frac{\int i dV}{2 \times m \times \Delta V \times v} \qquad \text{(S1)}$$

where i is the current (A), m is the mass of active materials (g), ΔV is the voltage window (V), and v is the scan rate (mV s^{-1}).

Batch-mode CDI tests.

For capacitive deionization (CDI) electrode preparation, each CDI electrode was prepared by pasting a mixture of the sample with carbon black and PVDF binder on graphite paper (thickness: 1 mm). The weight ratio of NC/rGO, carbon black, and PVDF is 8:1:1. The mixture was pressed onto graphite papers and dried in a vacuum oven at 60 °C overnight.

The CDI experiments were investigated by batch-mode electrosorption experiments with a continuously recycling system, as described in our previous work.[S2] In each experiment, the analytical NaCl solution was employed as the target solution with a volume of 20 mL, and the flow rate was 100 mL min^{-1}. A direct voltage from 0.8 to 1.2 V with an interval of 0.2 V was applied. The relationship between conductivity and concentration was obtained according to a calibration table made prior to the experiment.[S3] The concentration variation was continuously monitored and measured at the outlet of the unit cell by using an ion conductivity meter. The initial conductivity of NaCl solution was around 1000 μS cm^{-1}, which corresponds to a concentration of 589 mg L^{-1} of NaCl solution, and the temperature was kept at 27 °C during measurements. The corresponding desalination capacity (Λ, mg g^{-1}) was defined as:

$$\Lambda = (C_0 - C_e) \times V / m \qquad \text{(S2)}$$

where C_0 and C_e are the initial and final NaCl concentrations (mg L^{-1}), V is the volume of the NaCl solution (L), and m is the total mass of the electrode materials (g).

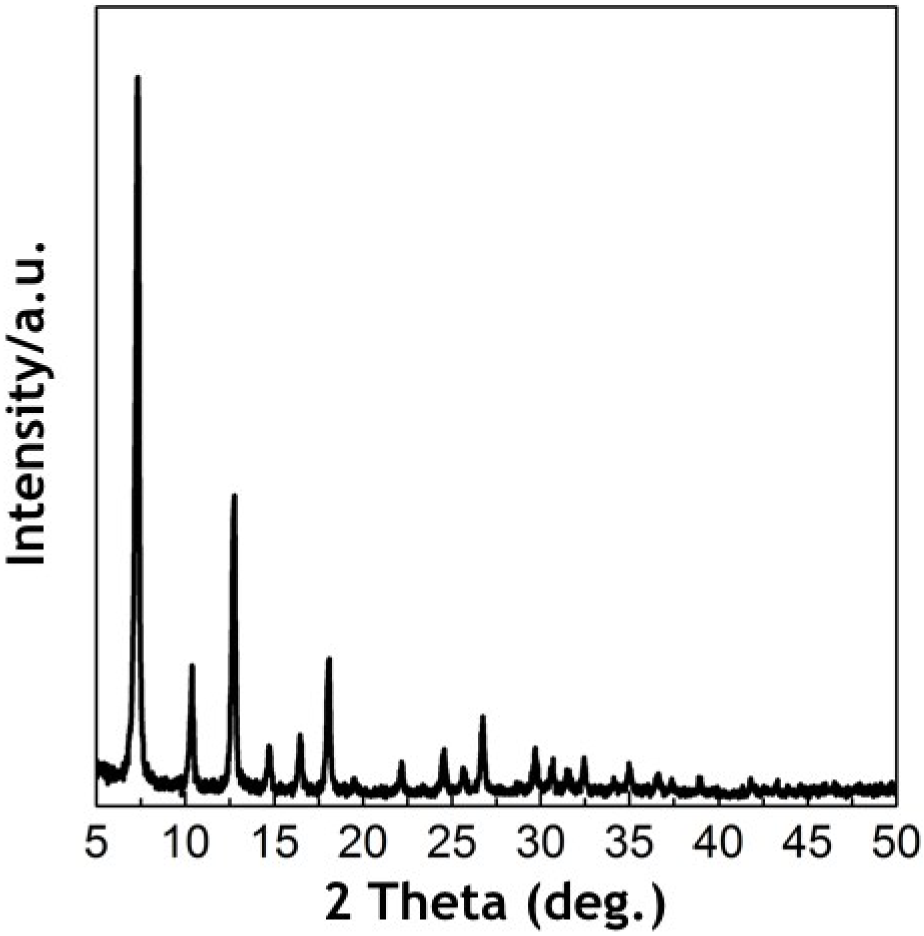

Fig. S1 XRD pattern of ZIF-8/GO.

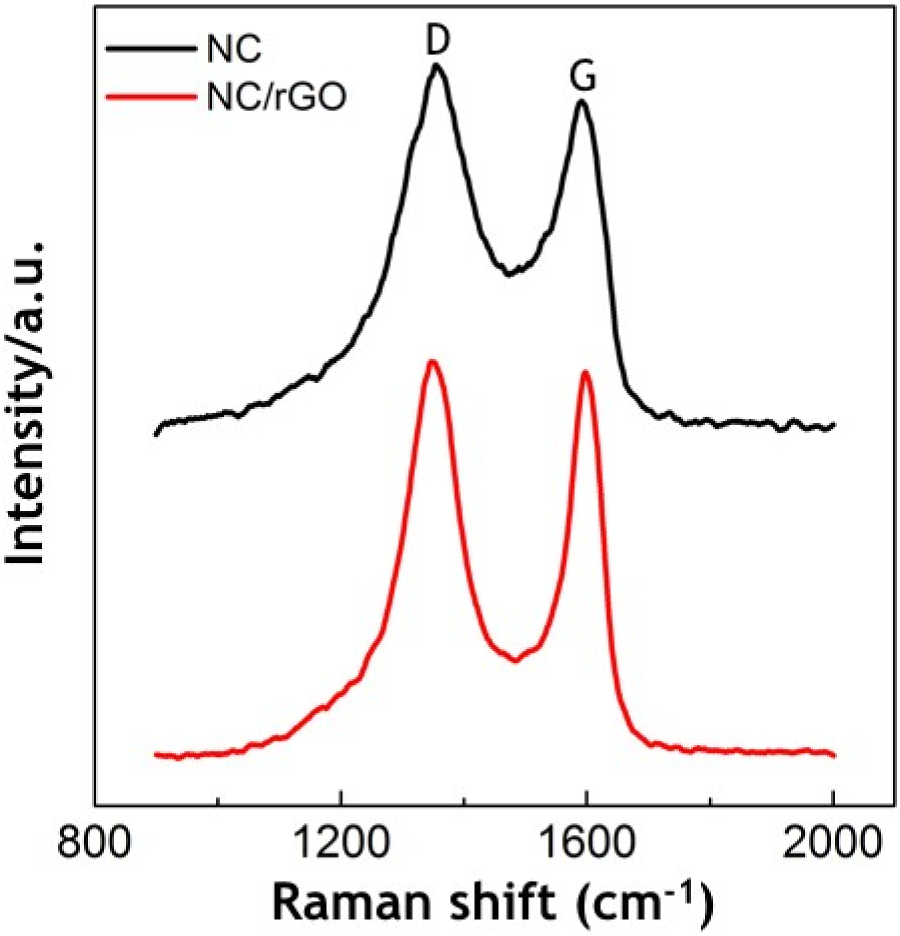

Fig. S2 Raman spectra of NC and NC/rGO.

Note 1: Raman spectra were further used to investigate the local structure of the porous carbons (**Fig. S2**). It can be seen that the two samples exhibit D- and G-bands centered at 1355 cm^{-1} and 1585 cm^{-1}, respectively, corresponding to sp^3-carbon in disordered carbon structures and sp^2-carbon in graphitic carbon structures.[S4] The relative ratio of the intensity of the G-band to that of the D-band (I_G/I_D) is usually representative of the degree of graphitization in porous carbons.[S5] Obviously, NC/rGO shows a higher I_G/I_D value (~0.95) than NC (~0.82), suggesting a higher degree of graphitization of NC/rGO.

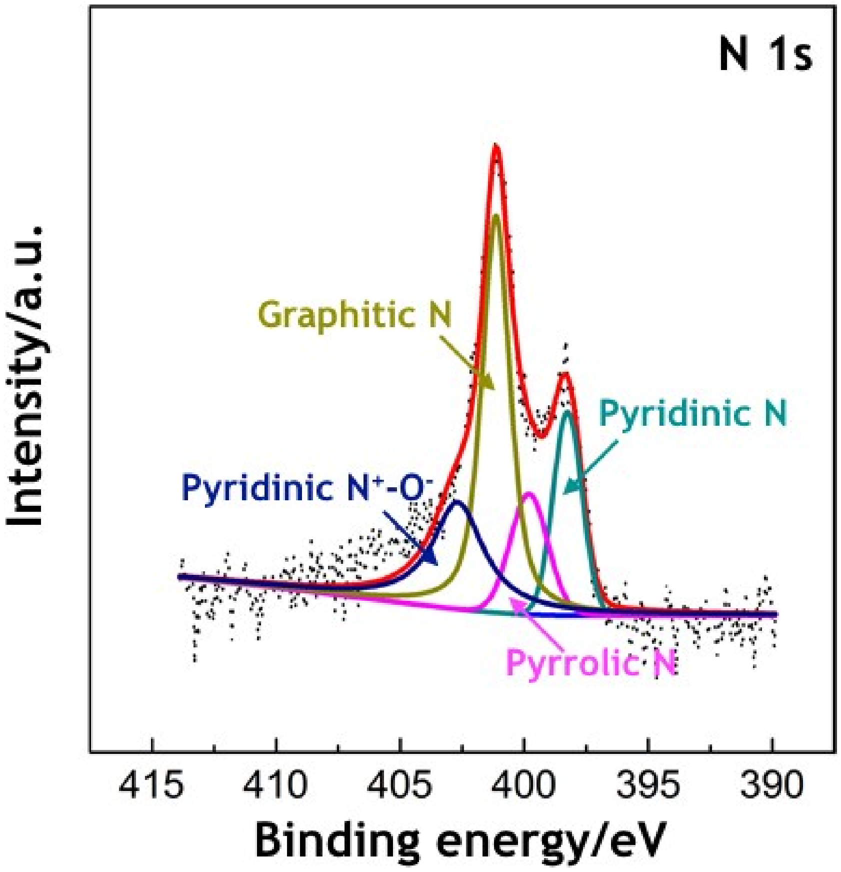

Fig. S3 High-resolution N 1s spectrum of NC/rGO.

Note 2: The nitrogen species of NC/rGO were measured by XPS analysis, as shown in **Fig. S3**. The N 1s spectrum can be divided into four peaks appearing at around 398.2, 399.5, 401.0, and 402.6 eV, which can be attributed to pyridinic-N, pyrrolic-N, graphitic-N, and oxidized-N, respectively. The pyridinic-N and pyrrolic-N located at the easily accessible edges of the carbon matrix can easily contribute to the total capacitance by the pseudocapacitive effect,[S6] and can increase the wettability of the porous carbon.[S2] Meanwhile, graphitic-N is favourable for improving the electrical conductivity of the carbon matrix.[S7]

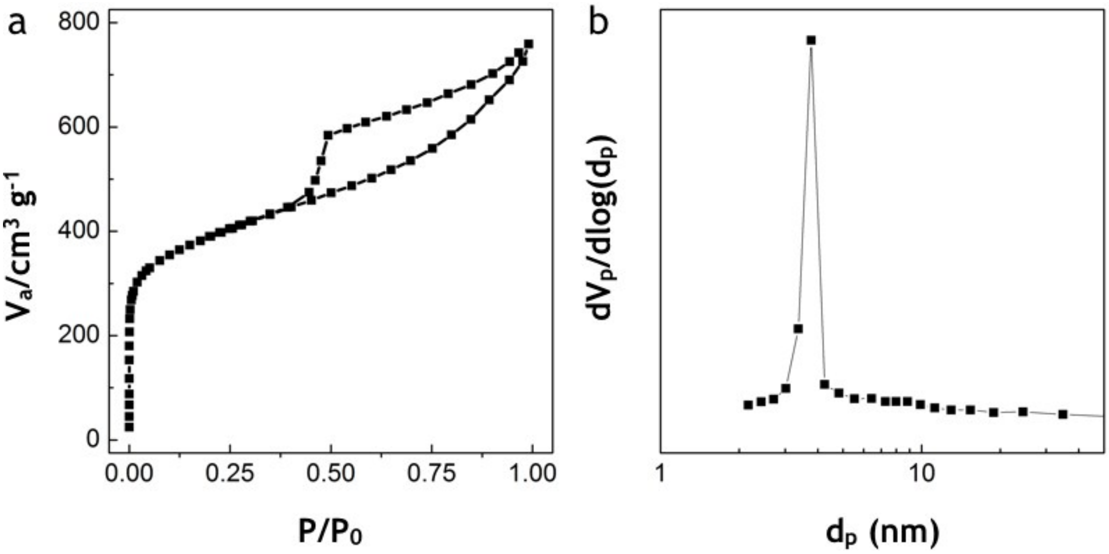

Fig. S4 (a) N_2 adsorption/desorption isotherm and (b) pore size distribution of NC/rGO.

Note 3: **Fig. S4** shows the N_2 adsorption/desorption isotherm and pore size distribution of NC/rGO. As shown in **Fig. S4a**, NC/rGO exhibits hybrid type I and IV isotherm with a sharp rise in the low relative pressure area (typical for micropores) and obvious capillary condensation in the mesopores.[S8] In addition, the pore size distribution of NC/rGO was obtained by using the Barrett-Joyner-Halenda model, which mainly reveals information on the mesopores. As shown in **Fig. S4b**, NC/rGO shows a mesoporous structure, which is believed to be beneficial for ion diffusion and accommodation during the low-voltage CDI process.[S9] The specific surface area of NC/rGO is calculated to be 1360 m^2 g^{-1}.

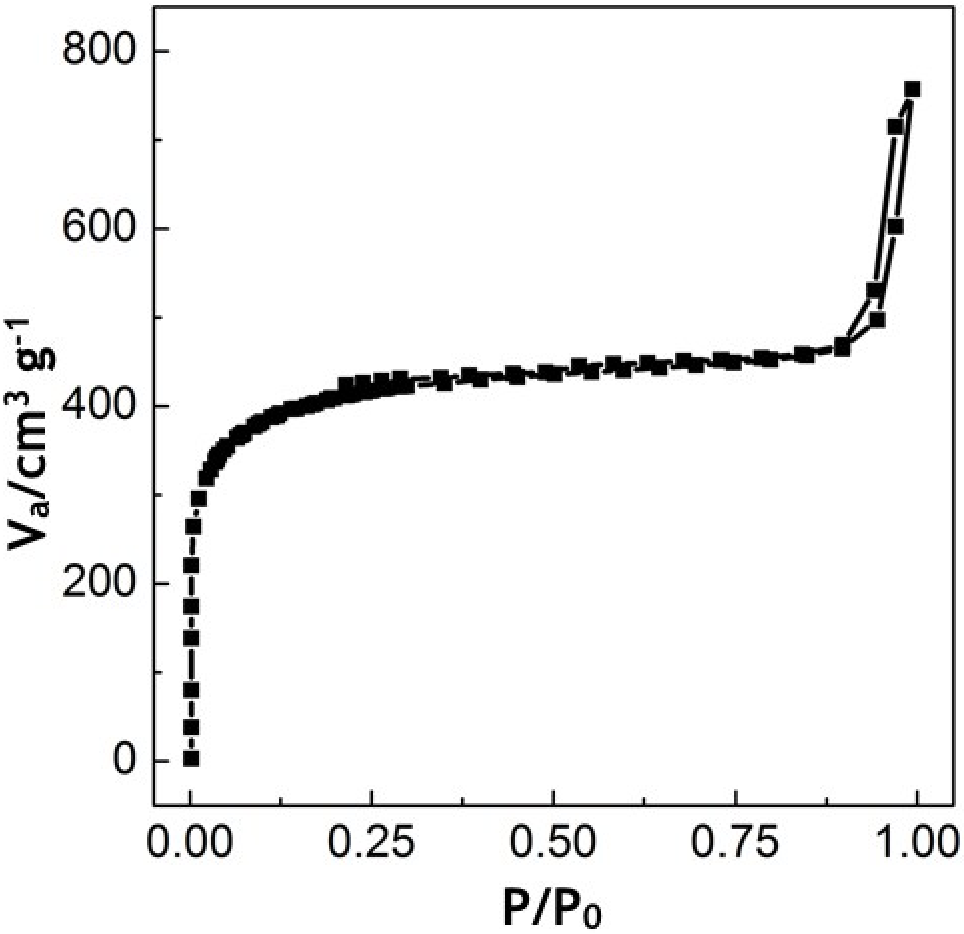

Fig. S5 N_2 adsorption/desorption isotherm of NC.

Note 4: The N_2 adsorption/desorption isotherm of NC (**Fig. S5**) shows a type I isotherm with a sharp rise at low relative pressure ($P/P_0 < 0.1$) and a slight uptake at high relative pressure ($P/P_0 > 0.9$), indicating that NC is a microporous material and that the presence of some macropores is possibly derived from the spaces between nanoparticles.[S5] The specific surface area of NC is calculated to be 1443 m^2 g^{-1}.

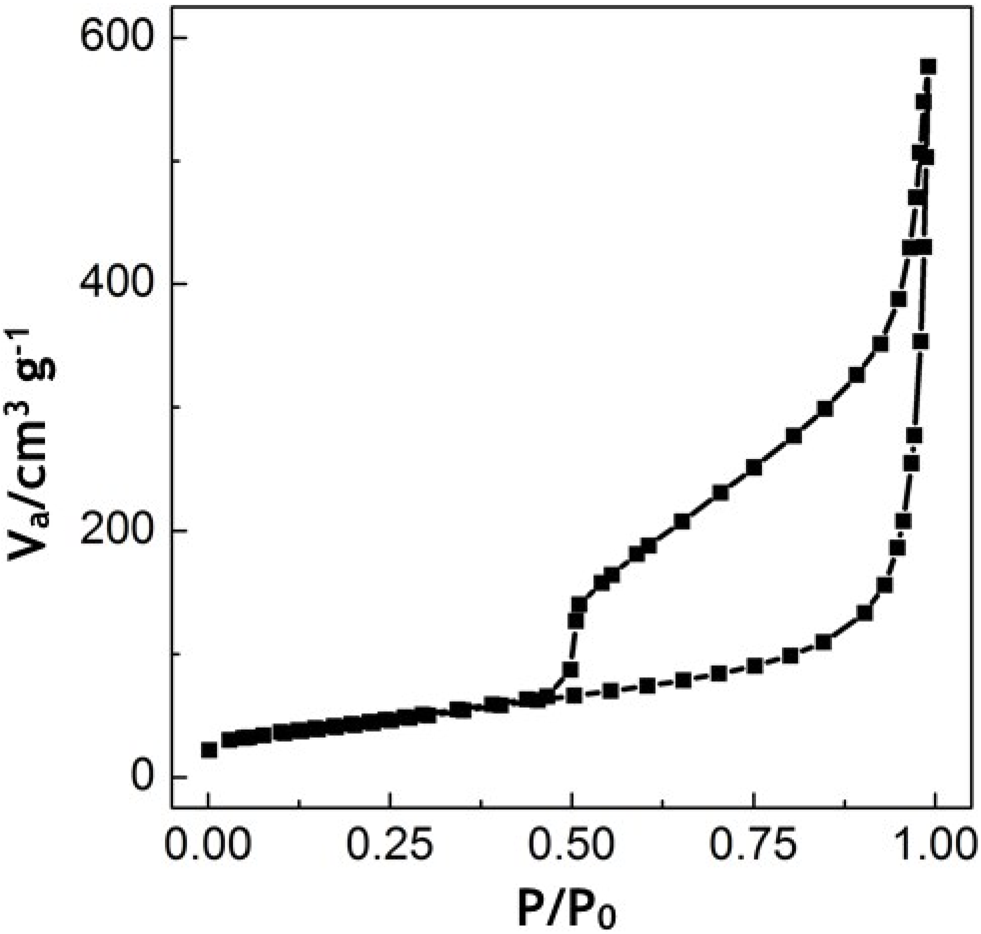

Fig. S6 N_2 adsorption-desorption isotherm of rGO.

Note 5: **Fig. S6** shows the N_2 adsorption-desorption isotherm of rGO. The specific surface area of rGO is calculated to be 150 m^2 g^{-1}.

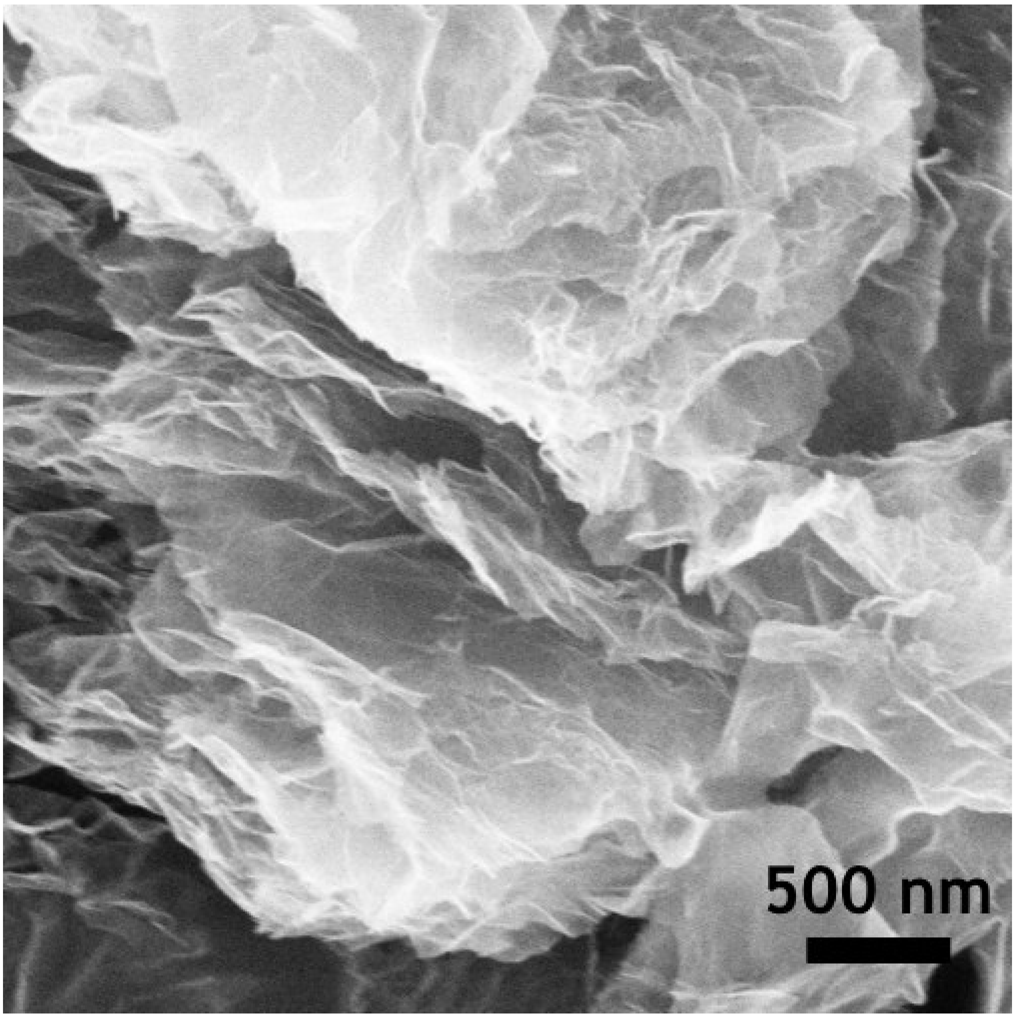

Fig. S7. FESEM image of rGO.

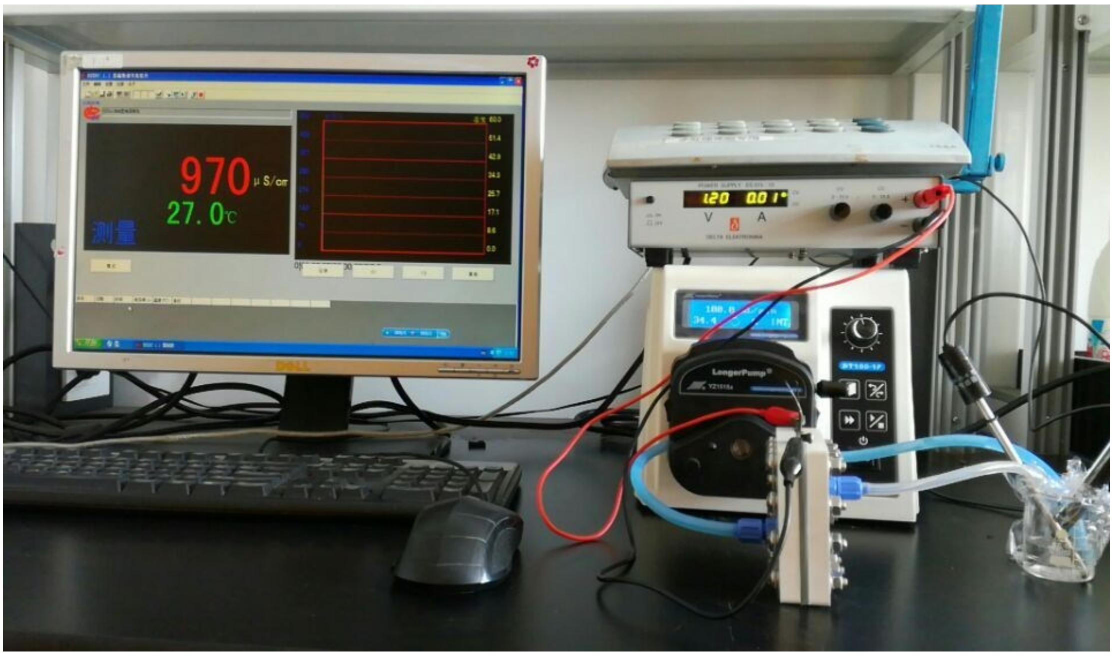

Fig. S8. Photograph of the CDI operation details.

Note 6: In each CDI electrochemical experiment, we used a NaCl solution with an initial conductivity of around 1000 μS cm^{-1}, which corresponds to a concentration of 589 mg L^{-1} of NaCl solution, as the target solution. The solution was continuously pumped from a peristaltic pump into the cell and then effluent returned to the unit cell, while the concentration variation was continuously monitored and measured at the outlet of the unit cell by using an ion conductivity meter. During the CDI process, charged ions are removed by electrosorption at the surface of polarized electrodes. Ions are entrapped at the electrode-solution interface by the formation of an electric double layer. During initial charging of the electrodes with a constant applied potential, ions migrate to the electrode-water interface, followed by EDL establishment as ions accumulate near the electrode surface. As ions accumulate, the electric field gradually vanishes in the bulk solution until equilibrium is attained. Then, the CDI cell was recycled by short-circuiting, while the NaCl concentration increased up to the initial value. This concentration variation was monitored and measured at the outlet of the unit cell by using an ion conductivity meter, and recorded by the software.

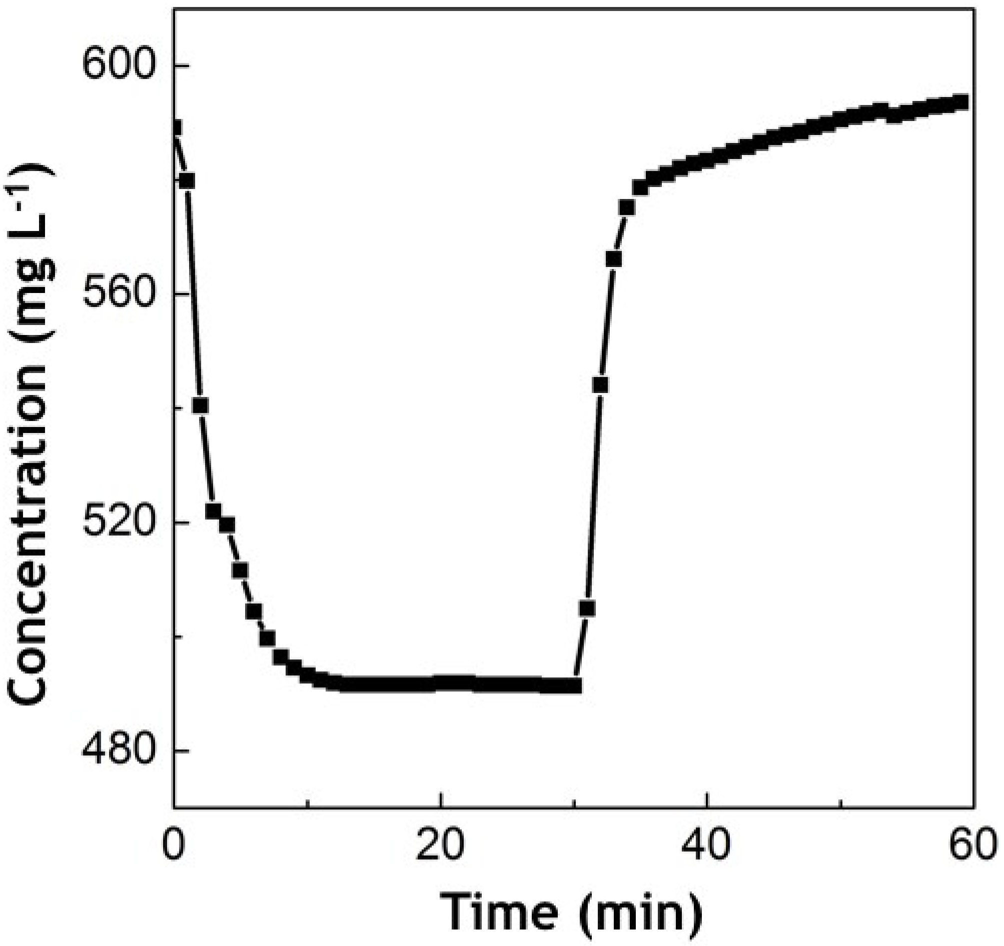

Fig. S9. NaCl concentration variation for pure NC.

Table S1. Comparison of NC/rGO with other graphene nanosheet (GN)-based hybrids.

Type	Specific surface area ($m^2\ g^{-1}$)	Voltage (V)	Desalination capacity ($mg\ g^{-1}$)	Ref.
GN/activated carbon	779	1.2	2.94	S3
GN/carbon nanotubes	438.6	1.2	1.4	S10
GN/mesoporous carbon	685.2	2.0	0.73	S11
GN/hollow carbon spheres	400.4	1.6	2.3	S12
GN/pyridine	--	2.0	0.88	S13
GN/hierarchically porous carbon	384.4	1.2	6.18	S14
GN/carbon nanotubes/activated carbon	426.6	1.2	10.94	S15
NC/rGO	1360	1.2	17.52	This work

References

S1. X. Xu, L. Pan, Y. Liu, T. Lu and Z. Sun, *J. Colloid Sci.*, 2015, **445**, 143-150.

S2. Y. Liu, X. Xu, M. Wang, T. Lu, Z. Sun and L. Pan, *J. Mater. Chem. A*, 2015, **3**, 17304-17311.

S3. H. Li, L. Pan, C. Nie, Y. Liu and Z. Sun, *J. Mater. Chem.*, 2012, **22**, 15556-15561.

S4. Y. Liu, T. Lu, Z. Sun, D. H. Chua and L. Pan, *J. Mater. Chem. A*, 2015, **3**, 8693-8700.

S5. W. Chaikittisilp, M. Hu, H. Wang, H.-S. Huang, T. Fujita, K. C.-W. Wu, L.-C. Chen, Y. Yamauchi and K. Ariga, *Chem. Commun.*, 2012, **48**, 7259-7261.

S6. B. Jiang, C. Tian, L. Wang, L. Sun, C. Chen, X. Nong, Y. Qiao and H. Fu, *Appl. Surf. Sci.*, 2012, **258**, 3438-3443.

S7. X. Xu, Z. Sun, D. H. Chua and L. Pan, *Sci. Rep.*, 2015, **5**, 11225.

S8. J. Tang, R. R. Salunkhe, J. Liu, N. L. Torad, M. Imura, S. Furukawa and Y. Yamauchi, *J. Am. Chem. Soc.*, 2015, **137**, 1572-1580.

S9. X. Xu, Y. Liu, M. Wang, X. Yang, C. Zhu, T. Lu, R. Zhao and L. Pan, *Electrochim. Acta*, 2016, **188**, 406-413.

S10. H. Li, S. Liang, J. Li and L. He, *J. Mater. Chem. A*, 2013, **1**, 6335-6341.

S11. D. Zhang, X. Wen, L. Shi, T. Yan and J. Zhang, *Nanoscale*, 2012, **4**, 5440-5446.

S12. H. Wang, L. Shi, T. Yan, J. Zhang, Q. Zhong and D. Zhang, *J. Mater. Chem. A*, 2014, **2**, 4739-4750.

S13. H. Wang, D. Zhang, T. Yan, X. Wen, L. Shi and J. Zhang, *J. Mater. Chem.*, 2012, **22**, 23745-23748.

S14. X. Wen, D. Zhang, T. Yan, J. Zhang and L. Shi, *J. Mater. Chem. A*, 2013, **1**, 12334-12344.

S15. G. Zhu, W. Wang, X. Li, J. Zhu, H. Wang and L. Zhang, *RSC Adv.*, 2016, **6**, 5817-5823.